scientific data

OPEN

DATA DESCRIPTOR

Bioclimatic indicators dataset for the orographically complex Canary Islands archipelago

Paula Sosa-Guillén ✉, Albano González, Juan C. Pérez, Francisco J. Expósito & Juan P. Díaz

The Canary Islands are an archipelago of significant natural value, with a large variety of endemic species living in them, making essential the study of the effects of climate change. This research is based on the use of dynamic techniques of climatic regionalisation to obtain climate projections that contribute to the conservation of ecosystems in the Canary Islands. In this work, climate projections derived from WRF simulations with a spatial resolution of 3 km were used to obtain a novel dataset of 53 bioclimatic indicators, called BICI–ULL (Bioclimatic Indicators in the Canary Islands, University of La Laguna). The regional climate simulations were driven by three CMIP5 models (GFDL–ESM2M, IPSL–CM5A–MR, and MIROC–ESM) over three periods (1980–2009, 2030–2059, 2070–2099) and two emission scenarios (representative concentration pathway 4.5 and 8.5), to obtain, among others, the standard climatic variables used to generate the bioclimatic indicators: temperature, precipitation, solar radiation, humidity and wind speed.

Background & Summary

Climate change is a globally significant phenomenon that has developed throughout Earth's history. The industrial revolution and the expansion of human activity brought with it the burning of fossil fuels and the massive release of greenhouse gases. This disrupted the climate and actively affected the planet's ecosystems. Many of the consequences of climate change are devastating for the Earth. As a result, the study of the global environment has become an essential resource for the preservation of the world's flora and fauna[1,2].

Specifically, islands are among the most vulnerable regions to climate change[3]. They are much more exposed, compared to continental areas, to rising sea levels, increases in air and water temperatures, heavy rains associated with cyclones[4], as well as intense wildfires[5] and wind speed enhancements. Furthermore, the biodiversity and endemism found in these regions, which often contain a variety of microclimates, are unique[6] and highly sensitive to abrupt climate changes[7].

Bioindices, biovariables, or bioclimatic indicators are extremely valuable resources that help to estimate the current state of an ecosystem and its possible future changes. In addition, they facilitate the projections of species migration and even serve to assess the environmental risks encountered in a specific region[8–10]. Some of the best known worldwide bioclimatic databases in the scientific community include WorldClim[11,12], CHELSA[13,14], CMCC-BioClimInd[15,16], CliMond[17,18], or TerraClimate[19].

WorldClim, one of the most widely used datasets, provides 19 biovariables at a spatial resolution reaching up to 30 arc-seconds, roughly 0.9 kilometers at the equator[11], with resolutions also available at 10, 5, and 2.5 minutes. This dataset encompasses climate data for both the recent past (1970–2000) and future projections (2021–2040, 2041–2060, 2061–2080, 2081–2100). To obtain gridded data for the recent past period weather station data were interpolated using thin-plate splines, using also some covariates: elevation, distance to the coast and MODIS satellite derived variables (maximum and minimum land surface temperature and cloud cover). For future periods the results of 23 Global Climate Models (GCMs), belonging to the Coupled Model Intercomparison Project Phase 6 (CMIP6)[20], were used. Firstly, the difference between the output of the GCM runs for the recent past period and for the selected future period is computed and it is interpolated to the high resolution grid. Then, these changes are applied to WorldClim data for the recent past. The authors assume that climate change signal is relatively stable over space, so it can be obtained from low resolution GCM data. The

Grupo de Observación de la Tierra y la Atmósfera (GOTA). Universidad de La Laguna. A/Astrofísico Francisco Sánchez s/n. 38200 La Laguna, Tenerife, España, Spain. ✉e-mail: paula.sosa.guillen.09@ull.edu.es

projected climate data has been computed for all four Shared Socio-Economic Pathways (SSPs) that drive the simulations supporting the Intergovernmental Panel on Climate Change's (IPCC) 6th Assessment Report (AR6).

The CHELSA dataset (in its last version 2.1) includes 19 worldwide biovariables at high resolution in diferent time periods. It uses downscaled reanalysis data for temperature and precipitation at a horizontal resolution of 30 arc-seconds. The temperature computation relies on a statistical downscaling method, based on mean lapse rates and elevation, while the precipitation algorithm incorporates geographic predictors, including wind fields, exposure, cloud cover, and boundary layer height, with subsequent bias adjustment. To estimate the projections, a methodology similar to that used by WorldClim was used, calculating the changes from the results of GCMs, interpolating them to the required resolution, and finally adding them to the data for the recent past. Five GCMs (UKESM1–0–LL, IPSL–CM6A–LR, GFDL–ESM4, MRI–ESM2–0, MPI–ESM1–2–LR) and three Shared Socioeconomic Pathways (SSP1–2.6, SSP3–7.0, SSP5–8.5) were used. Building upon the methodology of CHELSA, CanaryClim v1.0[21] is a dataset comprising the same 19 high-resolution bioclimatic variables adapted to the Canary Islands. This dataset, including historical (1979-2013) and future (2071–2100) periods, was generated through the downscaling of the CHELSA v1.2 model[13,14] for precipitation and temperature. The creation of CanaryClim v1.0 involved using data from meteorological stations and bias adjustment was applied using B-spline interpolation[22].

Although these datasets have contributed significantly to the generation of bioclimatic variables at a spatial resolution that can be applicable to studies in sensitive ecosystems, they still present some drawbacks in geographically complex regions where interpolation methods mask the heterogeneity of physical processes occurring at the local scale. For example, bioclimatic patterns derived from WorldClim data seem more related with orography than with the actual climatic features of a mountainous region[23]. However, the results of dynamic climate regionalisations, based on mesoscale atmospheric models, are able to take into account some of these processes and keep physically consistent relationships between the different meteorological variables. Furthermore, dynamic simulations must be performed with sufficient spatial resolution to account for the important effects of topography and different soil types. In previous studies[5,24,25] the authors have shown that in the Canary Islands the climatic variables vary sharply with the topography, which, for this region, is not consistent with the assumption that future changes vary smoothly over space.

This work introduces a unique dataset for the Canary Islands, called BICI–ULL (Bioclimatic Indicators in the Canary Islands by the ULL–GOTA). This dataset includes 53 biovariables derived from monthly temperature, precipitation, radiation, humidity, and wind speed averages over different periods calculated through dynamic regionalisation models. It uses boundary conditions from three global models (GFDL–ESM2M, IPSL–CM5A–MR, and MIROC–ESM) across three periods (1980–2009, 2030–2059, 2070–2099) and two CMIP5 scenarios (Representative Concentration Pathway, RCP 4.5 and 8.5), with a spatial resolution of 3 × 3 km. This project aims to improve our understanding of climate and its impacts on small, isolated regions with diverse ecosystems, providing valuable insights for the scientific community to enhance their knowledge in this field.

Methods

Raw data. The BICI−ULL dataset was generated from the monthly averaged series of temperature (at 2m from the surface), cumulative precipitation, humidity (at 2m from the surface), solar radiation (shortwave downwelling net flux), and wind speed (at 10m from the surface) available at the ULL research data repository website. Data are uploaded in Sosa-Guillén *et al.*[26]. The characteristics of these data are specified below.

Data generation. Regional climate simulations for the Canary Islands were conducted using the non-hydrostatic WRF model (WRF/ARW, v3.4.1) with a one-way triple nesting configuration, achieving a grid resolution of 3 × 3 km. The choice of WRF version and the selection of physical parameterisations were in line with prior studies in the same region[27,28]. Specifically, the chosen physics schemes encompassed the WRF double-moment 6-class microphysics scheme[29], the Yonsei University planetary boundary layer scheme[30], the Noah land surface model[31], and the Community Atmosphere Model version 3 scheme[32] for both longwave and shortwave radiation. Additionally, the Kain-Fritsch scheme[33] was used for cumulus parameterisation in the two outer domains. In the innermost domain, such parametrisation was deactivated, obtaining a convection-permitting simulation. The vertical resolution was structured with 32 vertical levels, distributed unevenly and mainly concentrated near the Earth's surface.

The boundary conditions driving the RCM simulations were obtained from three GCMs participating in the CMIP5 project, with their key attributes summarised in Table 1. From all the models that provide data to CMIP5, three were chosen that behaved adequately for the area of interest, based on the annual cycles and the simulation of the teleconnections[34], and that provided, at the time the simulations started, all the necessary variables at the appropriate levels and with a time resolution of 6 hours. In addition, given the importance of sea surface temperature in the climate simulation on such small islands so close to a continent, it was taken into account that this variable was correctly defined in the study area and that there were no problems with the land and ocean masks.

In all instances, only the r1i1p1 realisation was used during the downscaling procedure. To assess projected changes, three different periods were simulated: the recent past (1980–2009), the middle (2030–2059), and the end of the twenty-first century (2070–2099). The simulations started one year before the target period (spin-up time) to mitigate the physical inconsistencies arising from the mismatch between the low-resolution GCM initial conditions and the high-resolution RCM, thus excluding that year from the analysis. For the future periods, two different scenarios for greenhouse gas concentration were considered, namely the CMIP5 representative concentration pathway 4.5 and 8.5 (RCP4.5 and RCP8.5)[35]. The data, therefore, are grouped in 30-year periods and for two different scenarios, similar to how they are presented in the previously mentioned databases, such as

GCM name	Institution	Resolution	Reference
GFDL-ESM2M	Geophysical Fluid Dynamics. Laboratory, USA.	2.5° × 2°	Dunne *et al.*[50]
IPSL-CM5A-MR	Institut Pierre Simon. Laplace, France.	2.5° × 1.25°	Dufresne *et al.*[51]
MIROC-ESM	The University of Tokyo, National Institute for Environmental Studies, and Japan Agency for Marine-Earth Science and Technology, Japan.	2.8° × 2.8°	Watanabe *et al.*[52]

Table 1. CMIP5 GCMs used as initial and boundary conditions in the downscaling experiments.

WorldClim, CHELSA, or CanaryClim. This allows the analysis of the variability due to the three driving GCMs for each period. The reason for using these time periods, rather than continuous simulations from 1980 to 2099, and only three global models is the high computational cost of simulating at such high spatial resolution, which implies using a small simulation time step, specifically 12 seconds for the innermost domain. From the instantaneous values of the variables at these time intervals, the daily statistics (maximum, minimum, average) of some of the variables, such as temperature, humidity, wind, …, and the daily accumulated values of others, such as radiation or precipitation, are calculated at run time. Instantaneous and cumulative values are also stored hourly to study subdaily behaviours. From the daily values, monthly statistics are calculated and used as input data to compute the bioindices.

Bias adjustment. Despite the continuous enhancement of Regional Climate Models (RCMs) in terms of complexity and spatial resolution, the outcomes frequently exhibit discrepancies that can be assessed by comparing them with observed data[36]. These discrepancies often originate from the parent Global Climate Models (GCMs) that drive the RCMs. Hence, particularly in studies related to impact assessments, it is essential to implement a bias adjustment approach.

In this study, a specific bias adjustment technique known as the Scaled Distribution Mapping (SDM) algorithm, designed to preserve trends, was used[37]. To implement this method, the SDM code was sourced from the Python pyCAT package (available at https://github.com/wegener-center/pyCAT[38]). Since gridded data for the Canary Islands are only available for temperature and precipitation, the reference data for the bias adjustment were taken from a previous high-resolution WRF simulation[27] driven by ERA-Interim data. Therefore, these simulated data have been taken as a surrogate reality, instead of direct observations. Although the quality of the results of this reference simulation has been assessed in previous works[27,39,40], some biases still remain, which will be propagated to the adjusted data.

Bioindicators input data. Bioindicators are derived from the standard climate variables indicated in the Raw data section. These include: Mean, maximum, and minimum temperature (Tg, Tx, Tn), precipitation (Pr), shortwave downwelling net flux (Sr), relative humidity (Rh), and wind speed (Ws).

Initially, daily data for these variables are collected for each year within the designated period. Subsequently, monthly averages are computed (except for precipitation, where monthly accumulations are determined instead). This results in 12 data files for each year and for each climate variable. The input for calculating bioindicators in the developed software includes monthly averaged values of these variables across all years considered. The workflow, depicted in Fig. 1, proceeds as follows:

1. Daily data for each climatic variable is available for all months and years within the study period.
2. Monthly values are computed from the daily data for each year:
   - Monthly averages are calculated for mean, maximum, and minimum temperature, radiation, humidity, and wind speed.
   - Monthly accumulations are calculated for precipitation.
3. Monthly values are then aggregated across years, resulting in an average for each month (e.g., all January values, all February values, …).
4. The final input consists of 7 sets (one for each variable, see Table 2) of 12 files each, corresponding to the mean values of the selected month over the entire period.

From this point onwards, the monthly average values for the specified period are indicated as "12 months". These 7 × 12 files will be denoted by uppercase letters according to the variable: TG, TX, TN, PR, SR, RH, WS.

Bioclimatic indicators. The definition of the 53 BICI–ULL bioindicators, which are summarised and outlined in Table 3, are listed below. They represent key aspects of temperature, precipitation, radiation, humidity, and wind speed in the Canary Islands. WorldClim[11,12] serves as the reference dataset for the bioindicators 1–19 (BIO1–19), whereas BIO44–53 relies on the CMCC-BioClimInd[15] dataset. The remaining (BIO20–43) have been introduced in this study.

The intention is to provide a comprehensive description of each of these bioindicators, along with the procedure used for their generation and associated units of measurement. These bioindicators provide unique insights into the climatic conditions of specific regions within the archipelago, thereby contributing to a more comprehensive assessment of their climatic environment.

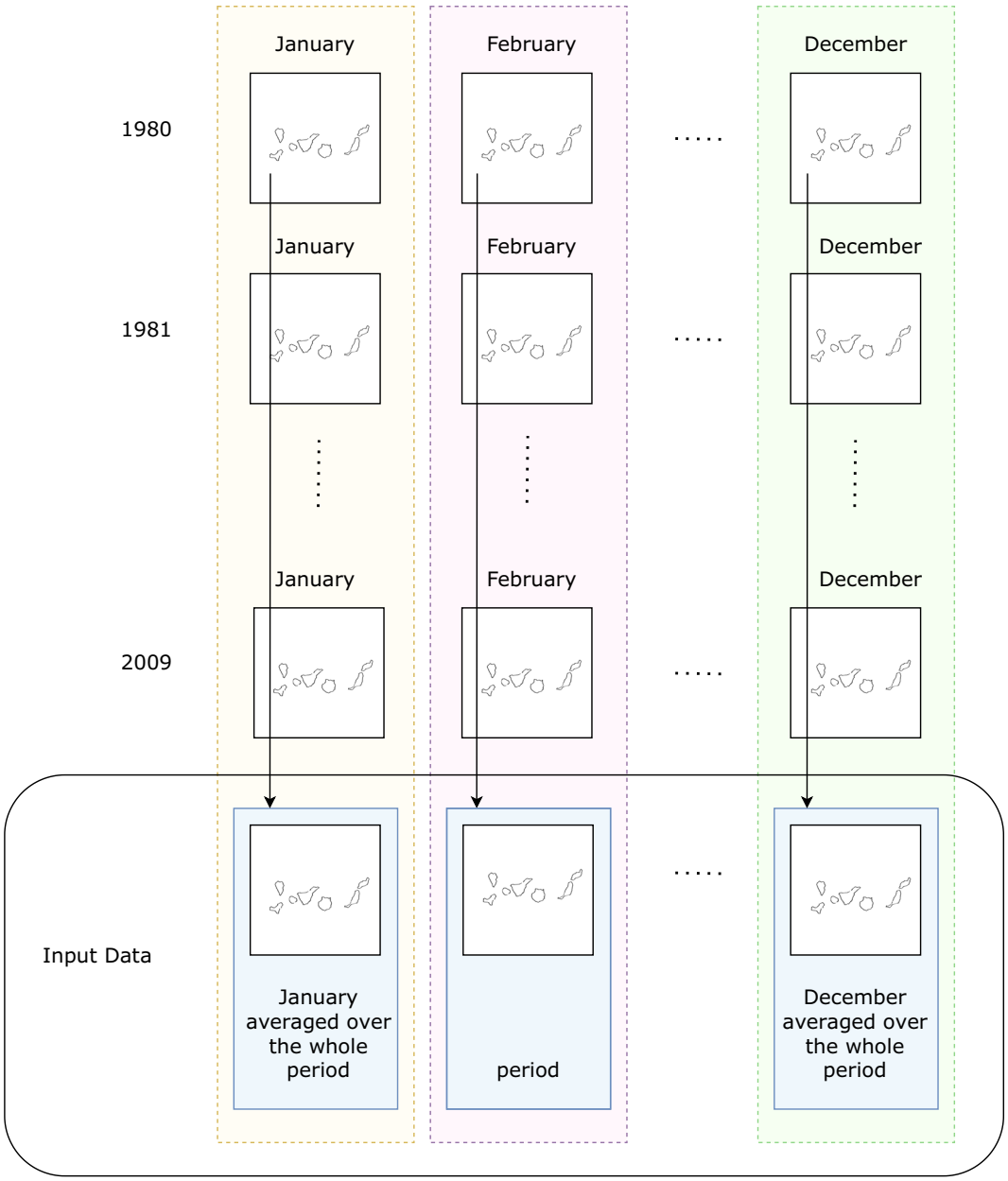

Fig. 1 Workflow to generate the bioindcators input. This scheme is executed for any of the climatic variables (Tg, Tx, Tn, Pr, Sr, Rh, or Ws) and for any period. Starting from 30 years of monthly data, these values are averaged per month, resulting in a set of 12 monthly averages spanning the entire period. Blue boxes represent TG, TX, TN, PR, SR, RH, or WS for the 12-month global period.

BIO1 Annual mean temperature. This indicator has been calculated as the average of the mean temperature for the 12 months of the period (TG). The units associated with BIO1 are degrees Celsius (°C).

BIO2 Mean diurnal range. This indicator is defined as the difference between the maximum and minimum temperatures recorded in a specific period (TX, TN). It is obtained by calculating the average of the two climatic variables for the 12 months independently, followed by the subtraction of them. The mean diurnal range provides information about temperature variability and is measured in degrees Celsius (°C).

BIO3 Isothermality. Isothermality is defined as the ratio between the averaged diurnal range and the temperature annual range for a specific period. This calculation has been performed as BIO2 / BIO7, multiplied by 100. This index captures temperature fluctuations through the comparison of diurnal variability with seasonal variation. It is expressed as a percentage (%), and uses the variables of mean, maximum, and minimum temperature (TG, TX, TN).

BIO4 Temperature Seasonality. Temperature seasonality is derived from the standard deviation of the mean temperature across the 12 months of the period (TG), multiplied by 100. This indicator quantifies the magnitude of temperature fluctuations throughout the year and is expressed in percentage (%).

Name	Short definition	Acron.	Unit
Mean temperature	The monthly mean of daily mean temperature averaged to the whole period	TG	°C
Maximum temperature	The monthly mean of daily maximum temperature averaged to the whole period	TX	°C
Minimum temperature	The monthly mean of daily minimum temperature averaged to the whole period	TN	°C
Precipitation	The monthly accumulated of daily precipitation averaged to the whole period	PR	mm
Solar Radiation	The monthly mean of daily mean shortwave downwelling net flux averaged to the whole period	SR	$W\,m^{-2}$
Relative Humidity	The monthly mean of daily relative humidity averaged to the whole period	RH	%
Wind Speed	The monthly mean of daily mean wind speed averaged to the whole period	WS	$m\,s^{-1}$

Table 2. List of the standard climate variables used as input in the code to obtain the BICI−ULL dataset. The first column records the standard climate variable names, the second column provides a brief definition, the third column specifies the acronym, and the fourth column details the units.

BIO5 Maximum Temperature of Warmest Month. This indicator is obtained from the maximum temperature (TX). For each grid cell on the map, this value corresponds to the highest temperature across the 12 months. It provides insights into maximum extreme thermal conditions. It is calculated in degrees Celsius (°C).

BIO6 Minimum Temperature of Coldest Month. This indicator is obtained from the minimum temperature (TN). For each grid point, this value corresponds to the lowest temperature across the 12 months. It offers information about minimum extreme thermal conditions. It is calculated in degrees Celsius (°C).

BIO7 Temperature Annual Range. Using the maximum and minimum temperatures (TX, TN), this indicator is defined as the difference between the maximum temperature of the warmest month and the minimum temperature of the coldest month, BIO5-BIO6. It serves as an indicator of fluctuations between monthly extreme temperatures and is expressed in degrees Celsius (°C).

BIO8 Mean Temperature of Wettest Quarter. For this indicator, the climatic variables of mean temperature and precipitation (TG, PR) are used. BIO8 represents the average of the mean temperature during the wettest quarter (the consecutive 3 months with the highest precipitation). The units associated with BIO8 are degrees Celsius (°C).

BIO9 Mean Temperature of Driest Quarter. For this indicator, the climatic variables of mean temperature and precipitation (TG, PR) are used. BIO9 represents the average of the mean temperature during the driest quarter (the consecutive 3 months with the lowest precipitation). The units associated with BIO9 are degrees Celsius (°C).

BIO10 Mean Temperature of Warmest Quarter. This indicator is based on the mean temperature (TG). BIO10 corresponds to the average of the mean temperature during the warmest quarter (the consecutive 3 months with the highest mean temperature). The units associated with BIO10 are degrees Celsius (°C).

BIO11 Mean Temperature of Coldest Quarter. For this indicator, the mean temperature (TG) is used. BIO11 represents the average of the mean temperature during the coldest quarter (the consecutive 3 months with the lowest mean temperature). The units associated with BIO11 are degrees Celsius (°C).

BIO12 Annual Precipitation. This indicator is calculated as the sum of precipitation over the 12 months of the period. It is defined as the total amount of water an ecosystem receives throughout a year. The units associated with BIO12 are millimeters (mm), and it uses the climatic variable of precipitation (PR).

BIO13 Precipitation of Wettest Month. This indicator is derived from precipitation (PR). For each grid cell, the value corresponding to the highest precipitation within the 12 months is obtained. It represents the greatest amount per month of precipitated water recorded in the year and is calculated in millimeters (mm).

BIO14 Precipitation of Driest Month. This indicator is obtained from precipitation (PR). For each grid point, the value corresponding to the lowest precipitation within the 12 months is obtained. It represents the smallest amount per month of precipitated water recorded in the year and is calculated in millimeters (mm).

BIO15 Precipitation Seasonality. Precipitation seasonality is derived as the ratio between the standard deviation and the mean of the precipitation across the 12 months of the entire period (PR), multiplied by 100. To avoid divisions by zero, 1 mm has been added to the denominator. This indicator measures the magnitude of precipitation changes throughout the year and is expressed in percentage (%).

BIO16 Precipitation of Wettest Quarter. This indicator uses precipitation (PR). BIO16 represents the sum of precipitation during the wettest quarter (the consecutive 3 months with the highest precipitation). The units associated with BIO16 are millimeters (mm).

BIO17 Precipitation of Driest Quarter. This indicator uses precipitation (PR). BIO17 corresponds to the accumulated precipitation during the driest quarter (the consecutive 3 months with the lowest precipitation). The units associated with BIO17 are millimeters (mm).

BIO18 Precipitation of Warmest Quarter. For this indicator, the climatic variables of mean temperature and precipitation (TG, PR) are used. BIO18 represents the accumulated precipitation during the warmest quarter (the consecutive 3 months with the highest mean temperature). The units associated with BIO18 are millimeters (mm).

BIO19 Precipitation of Coldest Quarter. For this indicator, the climatic variables of mean temperature and precipitation (TG, PR) are used. BIO19 corresponds to the accumulated precipitation during the coldest quarter (the consecutive 3 months with the lowest mean temperature). The units associated with BIO19 are millimeters (mm).

Bioindicator number	Short definition	Unit	Climatic variables used
BIO1	Annual Mean Temperature	°C	TG
BIO2	Mean Diurnal Range	°C	TX, TN
BIO3	Isothermality	%	TG, TX, TN
BIO4	Temperature Seasonality	%	TG
BIO5	Max Temperature of Warmest Month	°C	TX
BIO6	Min Temperature of Coldest Month	°C	TN
BIO7	Temperature Annual Range	°C	TX, TN
BIO8	Mean Temperature of Wettest Quarter	°C	TG, PR
BIO9	Mean Temperature of Driest Quarter	°C	TG, PR
BIO10	Mean Temperature of Warmest Quarter	°C	TG
BIO11	Mean Temperature of Coldest Quarter	°C	TG
BIO12	Annual Precipitation	mm	PR
BIO13	Precipitation of Wettest Month	mm	PR
BIO14	Precipitation of Driest Month	mm	PR
BIO15	Precipitation Seasonality	%	PR
BIO16	Precipitation of Wettest Quarter	mm	PR
BIO17	Precipitation of Driest Quarter	mm	PR
BIO18	Precipitation of Warmest Quarter	mm	TG, PR
BIO19	Precipitation of Coldest Quarter	mm	TG, PR
BIO20	Annual Mean Radiation	$W\,m^{-2}$	SR
BIO21	Radiation of the Highest Insolation Month	$W\,m^{-2}$	SR
BIO22	Radiation of the Lowest Insolation Month	$W\,m^{-2}$	SR
BIO23	Mean Radiation of Wettest Quarter	$W\,m^{-2}$	PR, SR
BIO24	Mean Radiation of Driest Quarter	$W\,m^{-2}$	PR, SR
BIO25	Mean Radiation of Warmest Quarter	$W\,m^{-2}$	TG, SR
BIO26	Mean Radiation of Coldest Quarter	$W\,m^{-2}$	TG, SR
BIO27	Radiation Seasonality	%	SR
BIO28	Annual Mean Humidity	%	RH
BIO29	Humidity of Most Humid Month	%	RH
BIO30	Humidity of Least Humid Month	%	RH
BIO31	Mean Humidity of Wettest Quarter	%	PR, RH
BIO32	Mean Humidity of Driest Quarter	%	PR, RH
BIO33	Mean Humidity of Warmest Quarter	%	TG, RH
BIO34	Mean Humidity of Coldest Quarter	%	TG, RH
BIO35	Humidity Seasonality	%	RH
BIO36	Annual Mean Wind Speed	$m\,s^{-1}$	WS
BIO37	Wind Speed of Windiest Month	$m\,s^{-1}$	WS
BIO38	Wind Speed of Least Windy Month	$m\,s^{-1}$	WS
BIO39	Mean Wind Speed of Wettest Quarter	$m\,s^{-1}$	PR, WS
BIO40	Mean Wind Speed of Driest Quarter	$m\,s^{-1}$	PR, WS
BIO41	Mean Wind Speed of Warmest Quarter	$m\,s^{-1}$	TG, WS
BIO42	Mean Wind Speed of Coldest Quarter	$m\,s^{-1}$	TG, WS
BIO43	Wind Speed Seasonality	%	WS
BIO44	Mean Temperature of Wettest Month	°C	TG, PR
BIO45	Mean Temperature of Driest Month	°C	TG, PR
BIO46	Mean Temperature of Warmest Month	°C	TG
BIO47	Mean Temperature of Coldest Month	°C	TG
BIO48	Simplified Continentality Index	°C	TG
BIO49	Ellenberg Quotient	$°C\,mm^{-1}$	TG, PR
BIO50	Sum of Annual Temperature	°C	TG
BIO51	Modified Thermicity Index	°C	TG, TX, TN
BIO52	Potential Evapotranspiration Hargreaves	mm	TX, TN
BIO53	Potential Evapotranspiration Thornthwaite	mm	TG

Table 3. List of the bioclimatic indicators employed in the development of the BICI–ULL dataset. The first column records the bioclimatic indicator number, the second column provides a brief definition, the third column specifies the units, and the fourth column details the climatic variables used to derive the bioindicator (with the acronyms listed in Table 2).

BIO20 Annual Mean Radiation. This indicator is calculated as the average of the solar radiation over the 12 months of the period (SR). It is defined as the mean amount of radiation an ecosystem receives throughout a year. The units associated with BIO20 are W m^{-2}.

BIO21 Radiation of the Highest Insolation Month. This indicator is derived from radiation (SR). For each grid point, the value corresponding to the highest radiation within the 12 months is obtained. It represents the greatest amount of monthly mean incident radiation recorded in the year and is calculated in W m^{-2}.

BIO22 Radiation of the Lowest Insolation Month. This indicator is obtained from radiation (SR). For each grid cell, the value corresponding to the lowest radiation within the 12 months is obtained. It represents the smallest amount of monthly mean incident radiation recorded in the year and is calculated in W m^{-2}.

BIO23 Mean Radiation of Wettest Quarter. For this indicator, the climatic variables of radiation and precipitation (SR, PR) are used. BIO23 represents the average radiation during the wettest quarter (the consecutive 3 months with the highest precipitation). The units associated with BIO23 are W m^{-2}.

BIO24 Mean Radiation of Driest Quarter. For this indicator, the climatic variables of radiation and precipitation (SR, PR) are used. BIO24 corresponds to the average radiation during the driest quarter (the consecutive 3 months with the lowest precipitation). The units associated with BIO24 are W m^{-2}.

BIO25 Mean Radiation of Warmest Quarter. For this indicator, the climatic variables of radiation and mean temperature (SR, TG) are used. BIO25 represents the average radiation during the warmest quarter (the consecutive 3 months with the highest mean temperature). The units associated with BIO25 are W m^{-2}.

BIO26 Mean Radiation of Coldest Quarter. For this indicator, the climatic variables of radiation and mean temperature (SR, TG) are used. BIO26 corresponds to the average radiation during the coldest quarter (the consecutive 3 months with the lowest mean temperature). The units associated with BIO26 are W m^{-2}.

BIO27 Radiation Seasonality. Radiation seasonality is determined by the ratio between the standard deviation and the mean of the incident radiation across the 12 months of the entire period (SR), multiplied by 100. This indicator measures the magnitude of radiation changes throughout the year and is expressed in percentage (%).

BIO28 Annual Mean Humidity. This indicator is calculated as the average of the mean relative humidity over the 12 months of the period (RH). It is defined as the mean amount of humidity an ecosystem exhibits throughout a year. The units associated with BIO28 are expressed in percentage (%).

BIO29 Humidity of Most Humid Month. This indicator is derived from relative humidity (RH). For each grid point, the value corresponding to the highest humidity within the 12 months is obtained. It represents the highest amount of humidity recorded in the year and is calculated in percentage (%).

BIO30 Humidity of Least Humid Month. This indicator is obtained from relative humidity (RH). For each grid cell, the value corresponding to the lowest humidity within the 12 months is obtained. It represents the lowest amount of humidity recorded in the year and is calculated in percentage (%).

BIO31 Mean Humidity of the Wettest Quarter. For this indicator, the climatic variables of relative humidity and precipitation (RH, PR) are used. BIO31 represents the average humidity during the wettest quarter (the consecutive 3 months with the highest precipitation). The units associated with BIO31 are expressed in percentage (%).

BIO32 Mean Humidity of the Driest Quarter. For this indicator, the climatic variables of relative humidity and precipitation (RH, PR) are used. BIO32 corresponds to the average humidity during the driest quarter (the consecutive 3 months with the lowest precipitation). The units associated with BIO32 are expressed in percentage (%).

BIO33 Mean Humidity of the Warmest Quarter. For this indicator, the climatic variables of relative humidity and mean temperature (RH, TG) are used. BIO33 represents the average humidity during the warmest quarter (the consecutive 3 months with the highest mean temperature). The units associated with BIO33 are expressed in percentage (%).

BIO34 Mean Humidity of the Coldest Quarter. For this indicator, the climatic variables of relative humidity and mean temperature (RH, TG) are used. BIO34 corresponds to the average humidity during the coldest quarter (the consecutive 3 months with the lowest mean temperature). The units associated with BIO34 are expressed in percentage (%).

BIO35 Humidity Seasonality. Humidity seasonality is determined by the ratio between the standard deviation and the mean of the relative humidity across the 12 months of the entire period (RH), multiplied by 100. This indicator measures the magnitude of humidity changes throughout the year and is expressed in percentage (%).

BIO36 Annual Mean Wind Speed. This indicator is calculated as the average of the wind speed over the 12 months of the period (WS). The units associated with BIO36 are meters per second (m s^{-1}).

BIO37 Wind Speed of Windiest Month. This indicator is derived from wind speed (WS). For each grid point, the value corresponding to the highest wind speed within the 12 months is obtained. It is calculated in meters per second (m s^{-1}).

BIO38 Wind Speed of Least Windy Month. This indicator is obtained from wind speed (WS). For each grid point, the value corresponding to the lowest wind speed within the 12 months is obtained. It is calculated in meters per second (m s^{-1}).

BIO39 Mean Wind Speed of Wettest Quarter. For this indicator, the climatic variables of wind speed and precipitation (WS, PR) are used. BIO39 represents the average wind speed during the wettest quarter (the consecutive 3 months with the highest precipitation). The units associated with BIO39 are meters per second (m s^{-1}).

BIO40 Mean Wind Speed of Driest Quarter. For this indicator, the climatic variables of wind speed and precipitation (WS, PR) are used. BIO40 corresponds to the average wind speed during the driest quarter (the consecutive 3 months with the lowest precipitation). The units associated with BIO40 are meters per second (m s^{-1}).

Model	Period	RCP	File name
GFDL-ESM2M	1980 – 2009	—	bio1_GFDL_HIST_1980_2009.nc
	2030–2059	4.5	bio1_GFDL_45_2030_2059.nc
		8.5	bio1_GFDL_85_2030_2059.nc
	2070–2099	4.5	bio1_GFDL_45_2070_2099.nc
		8.5	bio1_GFDL_85_2070_2099.nc
IPSL-CM5A-MR	1980–2009	—	bio1_IPSL_HIST_1980_2009.nc
	2030–2059	4.5	bio1_IPSL_45_2030_2059.nc
		8.5	bio1_IPSL_85_2030_2059.nc
	2070–2099	4.5	bio1_IPSL_45_2070_2099.nc
		8.5	bio1_IPSL_85_2070_2099.nc
MIROC-ESM	1980–2009	—	bio1_MIROC_HIST_1980_2009.nc
	2030–2059	4.5	bio1_MIROC_45_2030_2059.nc
		8.5	bio1_MIROC_85_2030_2059.nc
	2070–2099	4.5	bio1_MIROC_45_2070_2099.nc
		8.5	bio1_MIROC_85_2070_2099.nc

Table 4. Example of file labeling. File names are provided for the BIO1 case. The first column indicates the model used to drive the downscaling simulations, the second column specifies the period, the third column denotes the RCP if applicable (the historical period is indicated by the acronym HIST), and the fourth column specifies the proposed filename.

BIO41 Mean Wind Speed of Warmest Quarter. For this indicator, the climatic variables of wind speed and mean temperature (WS, TG) are used. BIO41 represents the average wind speed during the warmest quarter (the consecutive 3 months with the highest mean temperature). The units associated with BIO41 are meters per second ($m\,s^{-1}$).

BIO42 Mean Wind Speed of Coldest Quarter. For this indicator, the climatic variables of wind speed and mean temperature (WS, TG) are used. BIO42 corresponds to the average wind speed during the coldest quarter (the consecutive 3 months with the lowest mean temperature). The units associated with BIO42 are meters per second ($m\,s^{-1}$).

BIO43 Wind Speed Seasonality. Wind speed seasonality is determined by the ratio between the standard deviation and the mean of the wind speed across the 12 months of the entire period (WS), multiplied by 100. To prevent divisions by zero, 1 has been added to the denominator. This indicator measures the magnitude of wind speed changes throughout the year and is expressed in percentage (%).

BIO44 Mean Temperature of Wettest Month. This indicator is derived from the mean temperature and precipitation (TG, PR). For each grid point, the value corresponding to the average temperature of the wettest month (the month with the highest precipitation) is obtained. The units associated with BIO44 are degrees Celsius (°C).

BIO45 Mean Temperature of Driest Month. This indicator is obtained from the mean temperature and precipitation (TG, PR). For each grid point, the value corresponding to the average temperature of the driest month (the month with the lowest precipitation) is obtained. The units associated with BIO45 are degrees Celsius (°C).

BIO46 Mean Temperature of Warmest Month. This indicator is derived from the mean temperature (TG). For each grid point, the value corresponding to the average temperature of the warmest month (the month with the highest mean temperature) is obtained. The units associated with BIO46 are degrees Celsius (°C).

BIO47 Mean Temperature of Coldest Month. This indicator is obtained from the mean temperature (TG). For each grid cell, the value corresponding to the average temperature of the coldest month (the month with the lowest mean temperature) is obtained. The units associated with BIO47 are degrees Celsius (°C).

BIO48 Simplified Continentality Index. This climatic indicator is used to assess the temperature change between the warmest and coldest seasons and is obtained from the mean temperature (TG). It is calculated by subtracting the mean temperature of the warmest month from that of the coldest month, BIO46-BIO47. The units associated with BIO48 are degrees Celsius (°C).

BIO49 Ellenberg Quotient. Following the definition provided by Ellenberg, 1963[41], this indicator is defined relating the temperature of the warmest month to the annual precipitation. BIO49 uses the climatic variables of mean temperature and precipitation (TG, PR). The ratio between these two indicators (BIO46 / BIO12) is calculated and multiplied by 1000, expressed in degrees Celsius per millimeter ($°C\,mm^{-1}$).

BIO50 Sum of Annual Temperature. This indicator, defined in Noce *et al.*[15], is calculated as the sum of the monthly mean temperature (TG) for all months of the year. The units associated with BIO50 are degrees Celsius (°C).

BIO51 Modified Thermicity Index. This indicator is defined based on Rivas-Martinez *et al.*[42] and the modification made in Noce *et al.*[15], where BIO51 is understood as the sum of the annual mean temperature (BIO1), the maximum temperature of the warmest month (BIO5), and the minimum temperature of the coldest month (BIO6). The unit associated with BIO51 is degrees Celsius (°C), and the climatic variables of mean, maximum, and minimum temperature (TG, TX, TN) are used for its computation.

BIO52 Potential Evapotranspiration Hargreaves. This indicator computes the potential evapotranspiration (PET) based on the definition outlined in Hargreaves *et al.*[43] and Hargreaves *et al.*[44]. PET is calculated for each individual month, and then, to determine the bioclimatic indicator, the annual accumulation is computed.

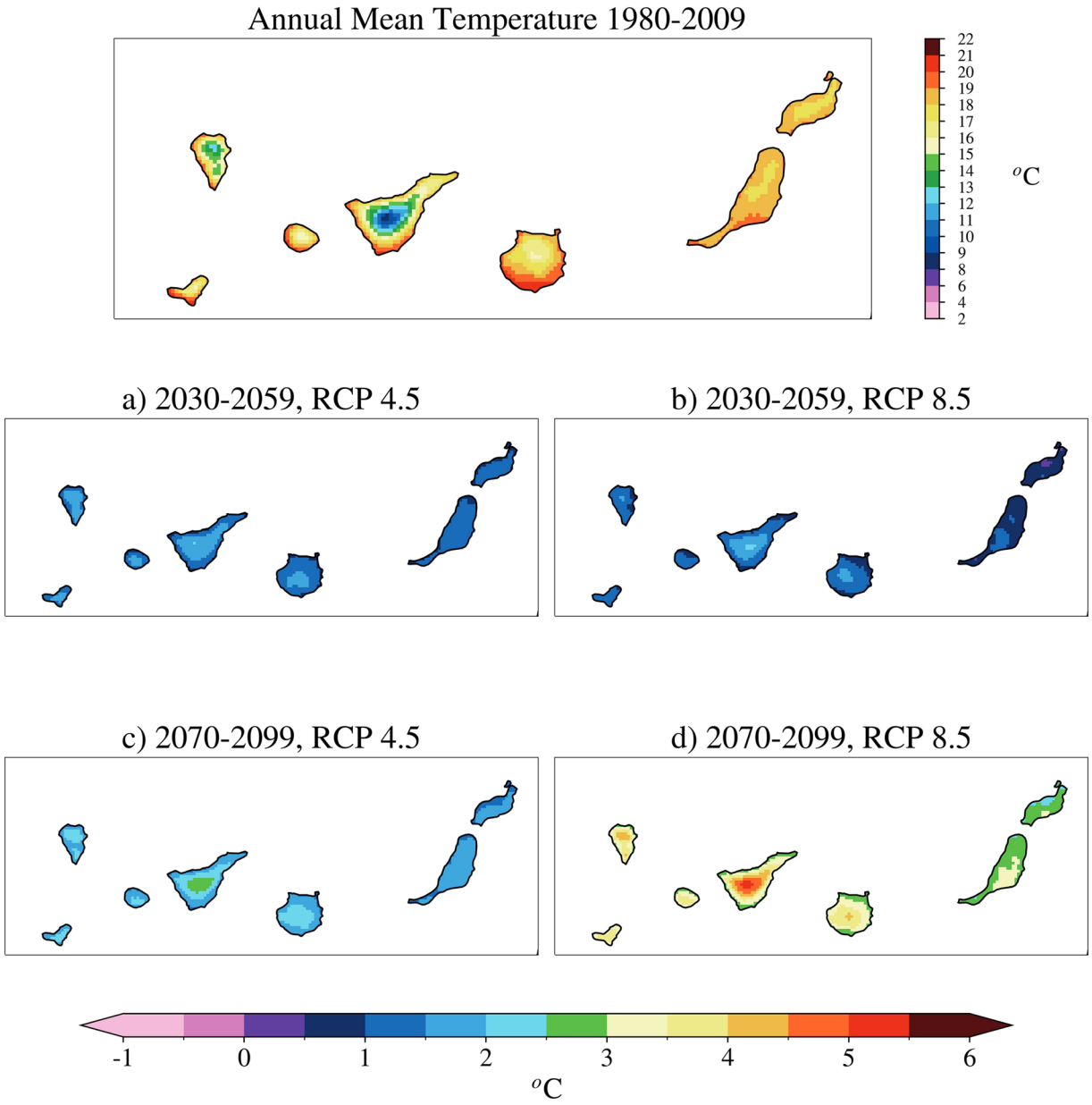

Fig. 2 Annual mean temperature of BICI–ULL dataset for the historical period along with its corresponding absolute change in different future scenarios, all for the simulations driven by the IPSL–CM5A–MR global model. *Top panel*: BIO1 for the period 1980–2009 in degrees Celsius (°C). *Bottom panels*: Absolute changes in BIO1 between the historical period (1980–2009) and the periods: (**a**) 2030–2059 RCP 4.5, (**b**) 2030–2059 RCP 8.5, (**c**) 2070–2099 RCP 4.5, (**d**) 2070–2099 RCP 8.5.

BIO52 uses the climatic variables of maximum and minimum temperature (TX, TN) and is expressed in millimeters (mm).

BIO53 Potential Evapotranspiration Thornthwaite. This indicator calculates the potential evapotranspiration (PET) using the definition proposed by Thornthwaite, 1948[45]. PET is calculated for each individual month, and then, to determine the bioclimatic indicator, the annual accumulation is computed. BIO53 employs the climatic variable of mean temperature (TG) and is expressed in millimeters (mm).

Data Records

The complete BICI–ULL dataset is available through the research data repository of the University of La Laguna in Sosa-Guillén *et al.*[26]. It consists of 795 files in NetCDF4 format with a grid cell resolution of 3 × 3 km covering the region of the Canary Islands. The files represent 53 bioclimatic indicators calculated in 30-year intervals for the periods: 1980–2009, 2030–2059, and 2070–2099, under the Representative Concentration Pathway (RCP) scenarios RCPs 4.5 and 8.5. The non-hydrostatic WRF model, with boundary conditions from three global models (see Table 1), was used to perform the simulations. The grid dimensions are (186 × 77), with 14322 points

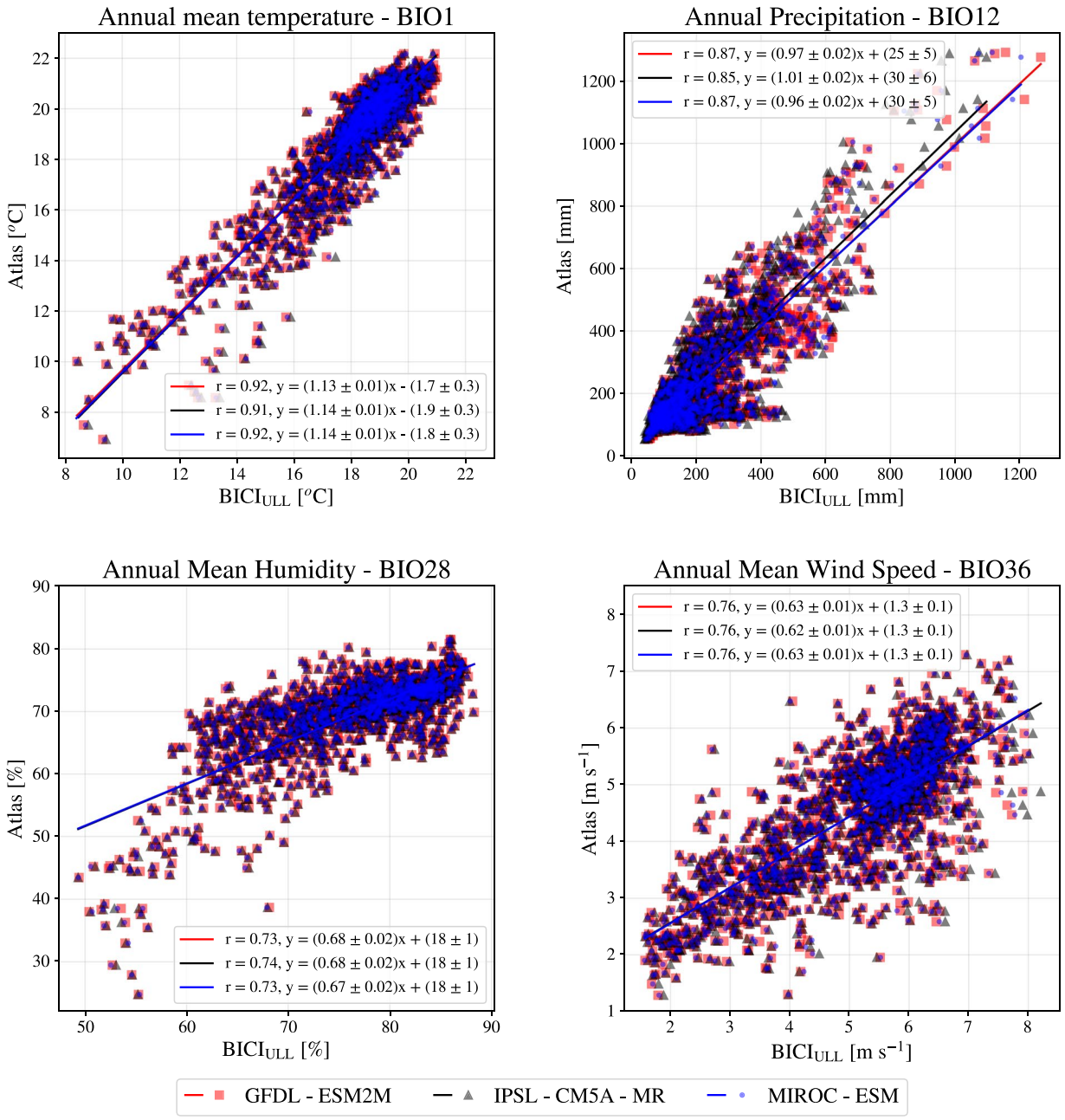

Fig. 3 Scatter plot comparing the main biovariables (BIO1, 12, 28, and 36) between BICI–ULL and the Digital Interactive Atlas for the Canary Islands[46]. The red color is associated with the GFDL–ESM2M, black with IPSL–CM5A–MR, and blue with MIROC–ESM model driven simulations for the recent past period. Squares, triangles, and dots represent the values obtained for BICI–ULL biovariables at each land grid point compared to those obtained in Atlas. The lines in each plot are the linear fits for each simulation, and the legend shows the associated equation in each case and the Pearson coefficient.

in total. It covers a longitude range of 18.3°W to 13.3°W and a latitude range of 27.5°N to 29.6°N, although the biovariables are only calculated for land cells. The name for all variables in the files is set for each bioindicator as shown in Table 3. The files comply with the conditions of the CF conventions for climate and forecast metadata designed to promote the processing and exchange of files created with the netCDF4 Application Programmer Interface.

The names associated with each file follow the format: bio*x*_*model*_*rcp*_*yini*_*yend*.nc. Here, *x* represents the number of the climatic indicator; *model* makes reference to the Global Circulation Model used as initial and boundary conditions for the regionalsation simulations and can be GFDL, IPSL, or MIROC, depending on whether it corresponds to GFDL–ESM2M, IPSL–CM5A–MR, or MIROC–ESM, respectively; the *rcp* indicates the forcing scenario, RCP 4.5 or RCP 8.5, or it will be defined as 'HIST' in the case of the historical period. Finally, *yind* and *yend* represent the years of the period, with *ini* identifying the first year of the period and *end*

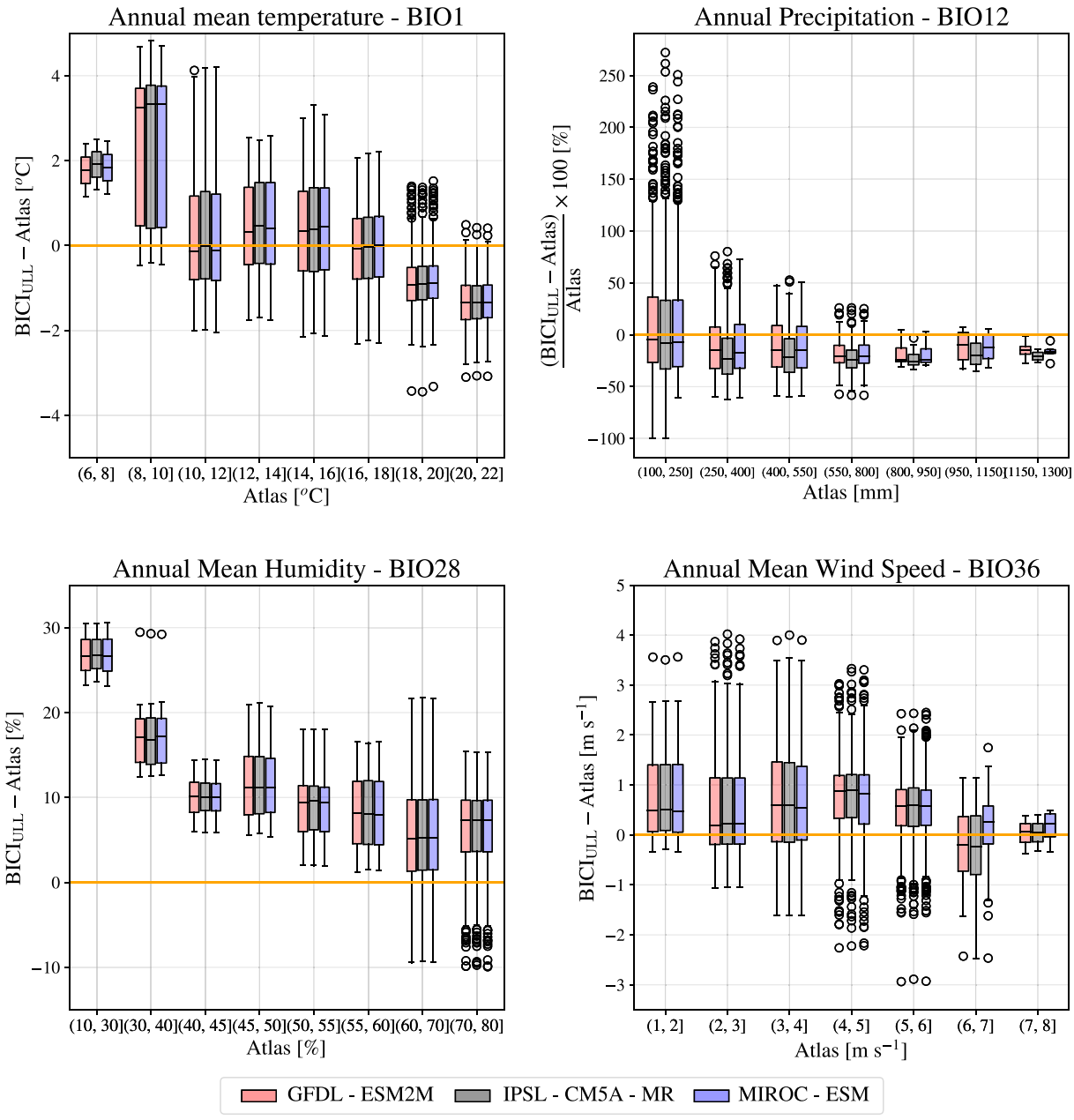

Fig. 4 Box plot comparing the main biovariables (BIO1, 12, 28, and 36) between BICI–ULL and the Digital Interactive Atlas of the Canary Islands[46]. The absolute error given is with respect to the dataset based on observations (Atlas), except for the case of annual cumulative precipitation, where reference is made to relative error. The color red is associated with the simulation driven by the GFDL–ESM2M model, black with IPSL–CM5A–MR, and blue with MIROC–ESM. The boxes extend from the first quartile (Q1) to the third quartile (Q3) of the data within the considered range. The black line inside the boxes represents the median of the data. The whiskers extend from the boxes by a factor of 1.5 within the inter-quartile range (IQR between Q1 and Q3). Black circular points are outliers, and the orange horizontal line is associated with 0, where the data are equal for both datasets, meaning BICI–ULL = Atlas, indicating no absolute or relative errors.

identifying the last year. In Table 4, an example of labeling for the first bioclimatic variable (BIO1) is shown, and the same scheme is followed for the remaining.

In Fig. 2, the annual mean temperature changes for the IPSL-CM5A-MR WRF model driven simulation and for the two considered periods and scenarios are shown. This image is an example of data representation obtained in this study. Expected temperature increases are highly dependent on elevation, being milder in coastal areas, which are more influenced by the ocean. This fact is very relevant for studies related to the distribution of some species in this region, since a mere vertical displacement of these species may not be feasible, as climatic variables vary differently depending on the topography.

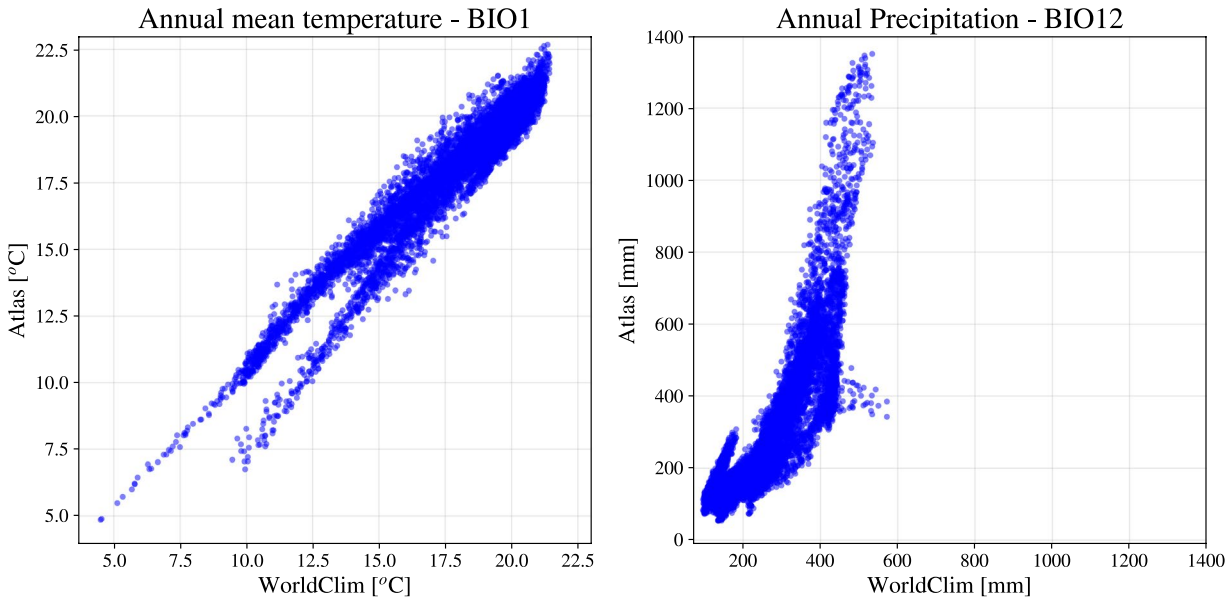

Fig. 5 Scatter plots comparing the main biovariables (BIO1 & 12, left and right, respectively) between WorldClim 2.0 and the Digital Interactive Atlas for the Canary Islands[46]. Blue dots represent the values obtained for WorldClim 2.0 biovariables at each pixel compared to those obtained in Atlas.

Technical Validation

In order to evaluate the uncertainties of this dataset obtained from the results of the dynamic regionalisation simulations carried out for the Canary Islands region, these indices have been compared with their equivalents obtained either from observations or from other existing datasets.

Comparison of BICI-ULL with the Digital Interactive Atlas for the Canary Islands. In this case, 45 out of the 53 biovariables obtained from the original data of the Climatic Atlas of the Canary Islands[46] (performed by Physical Geography and Environment Group (GFyMA) of the University of Las Palmas de Gran Canaria) were compared with the BICI–ULL dataset.

The Climatic Atlas of the Canary Islands (hereafter, Atlas) includes temperature (minimum, maximum, and mean), precipitation, relative humidity, and wind speed variables obtained from meteorological stations in the Canary Islands. Variables related to radiation were excluded from the comparison, as the Atlas lacks this variable and instead includes information on cloudiness. The dataset covers 50 years and has undergone correction and debugging processes (filtering and homogeneity adjustment) before entering the interpolation phase, performed using a multiple linear interpolation enriched with geographical information. Further details regarding the methodology employed in this work can be found in Luque Söllheim *et al.*[47].

The resolution of the Atlas is 100 × 100 meters for all variables, whereas the data used to obtain the BICI–ULL has a resolution of 3 × 3 km. Therefore, the resolution was degraded from 100 × 100 m to 3 × 3 km through the Climate Data Operators (CDO) using the conservative interpolation technique[48].

One noteworthy aspect is that in this Atlas, the series for minimum, maximum, and mean temperatures cover the period 1991–2020. Meanwhile, for precipitation, the start dates of the analysis differ for each of the islands. Thus, the series for the islands of La Palma, El Hierro, and Tenerife begin in 1975, for the island of La Gomera it starts in 1980, and for the three eastern islands in 1970; all concluding in 2020. For relative humidity, the period analysed is 1991–2020 for the islands of Tenerife and Gran Canaria, while for the remaining, the years 1991–2018 are studied. Finally, the considered period for wind speed ranges from 2001 to 2020. However, for the data used to obtain the BICI–ULL variables, the historical period of 1980–2009 is used, leading to an initial discrepancy between the analysis dates in the datasets.

For each of the biovariables, scatter plots like those shown in Fig. 3 were generated. Specifically, these plots present the results related to biovariables 1, 12, 28, and 36, corresponding to annual mean temperature, cumulative precipitation, relative humidity, and wind speed. These biovariables represent fundamental indicators, corresponding to the original variables. As observed, a high correlation is obtained for BIO1 and 12, always exceeding $r = 0.85$. For BIO36 and 28, the correlation coefficient is above 0.73. It is important to note that for wind speed, there are only 8 overlapping years for the periods used in Atlas and in BICI–ULL. Scatter plots for all biovariables, except for radiation, are presented and discussed in the Supplementary Information.

Figure 4 displays box plots comparing the two datasets for all the land grid points. In general, the results show a similar behaviour, although discrepancies are present, which can be attributed, in addition to the limitations of the simulations themselves and the bias adjustment method used, to various factors explained below.

Interpolating data is inherently challenging when comparing climatic data. The Atlas is generated through an interpolation that carries initial uncertainties, and further interpolation is applied to reduce resolution. In geographical regions characterised by high spatial variability, such as coastal or mountainous areas, the

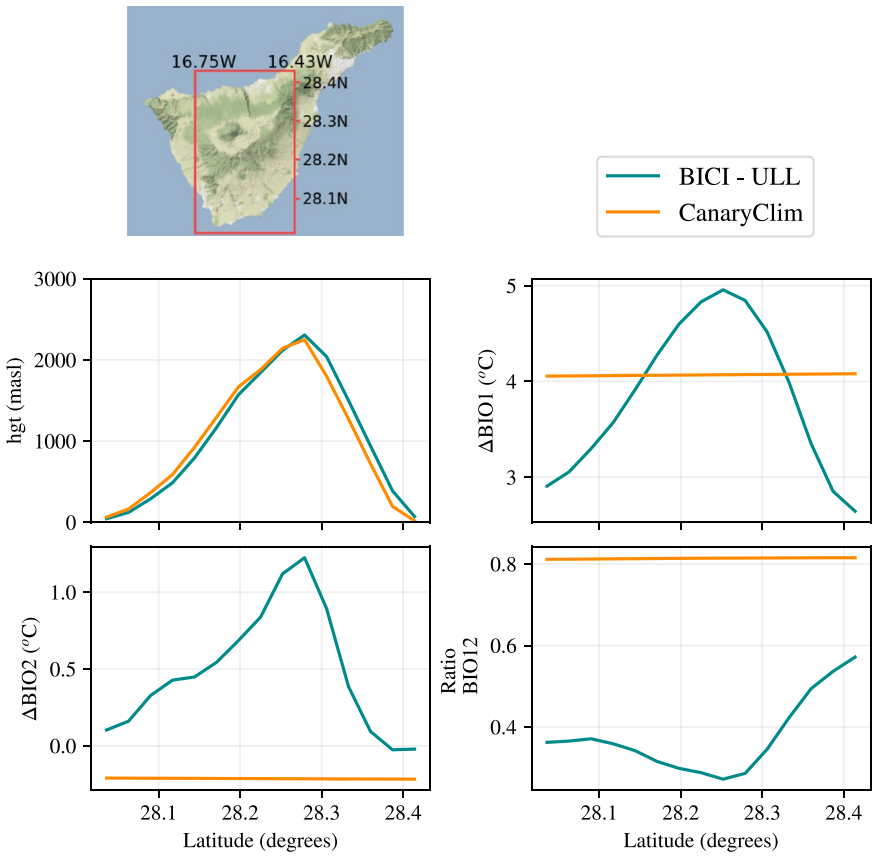

Fig. 6 Changes between BICI–ULL and CanaryClim v1.0[21] in the zonal average of BIO1, BIO2, and BIO12 corresponding to the transect indicated on the map for projected changes at the end of the 21st century. For BICI–ULL, data correspond to WRF simulations driven by the IPSL–CM5A–MR model using the RCP8.5 scenario. For CanaryClim v1.0, data correspond to IPSL–CM6A–LR in the SSP585 scenario. *Hgt* indicates terrain height in meters above sea level as considered in the corresponding dataset (masl). *ΔBIO1* represents the change in annual mean temperature, *ΔBIO2* indicates the change in mean temperature diurnal range, and *Ratio BIO12* refers to the annual precipitation ratio. Latitude ranges from 28.0°N to 28.41°N and the central longitude is 16.58°W.

interpolation process results in data degradation that must be taken into account. The proposed resolution in this work (3 x 3 km), results in terrain representation that may lead to steps up to 600 meters between neighboring cells in orographically complex areas. This fact conditions the accuracy of the models to represent the physical processes in that area. Therefore, in the steeper regions, where these altitude gradients are more important, it is expected that appreciable discrepancies will appear between the observed and modeled values, especially in variables such as temperature. A similar argument can be applied to those grid cells that include coastal zones. The resolution of the numerical model causes that the physical processes simulated in these pixels cannot be accurately resolved, which introduces uncertainties in the values obtained for the different climatic variables. Thus, the largest differences, of up to two degrees Celsius, occur in the higher regions (colder areas) and in the coast (the warmer zones). A similar situation occurs for humidity, even more pronounced due to the quasi permanent thermal inversion present in this region of the Atlantic, which determines the low humidity values registered in the upper areas of the islands.

From the results shown, it is also worth noting that precipitation exhibits larger differences between the two datasets as rainfall decreases. As the differences are expressed in percentages, the largest differences appear in areas with low precipitation, although they correspond to relatively low absolute differences. In general, the results of the three simulations slightly underestimate the observed precipitation and overestimate the average wind speed.

Comparison of WorldClim 2.0 Dataset with the Digital Interactive Atlas for the Canary Islands. One of the most widely used databases worldwide is WorldClim[11,12]. However, despite its relevance, a direct comparison between BICI–ULL and WorldClim has not been performed in this work, since, as will be shown below, it does not provide as accurate data for precipitation as the other analysed databases. Therefore, to take into account the behavior of WorldClim against observational data in the Canary Islands, this section compares this dataset with the Climatic Atlas of the Canary Islands.

WorldClim 2.0 was used at its maximum resolution (30 arc-seconds) for the recent past period (1970–2000). The analysis focused on biovariables 1 and 12 (Fig. 5), the most relevant variables available in WorldClim 2.0.

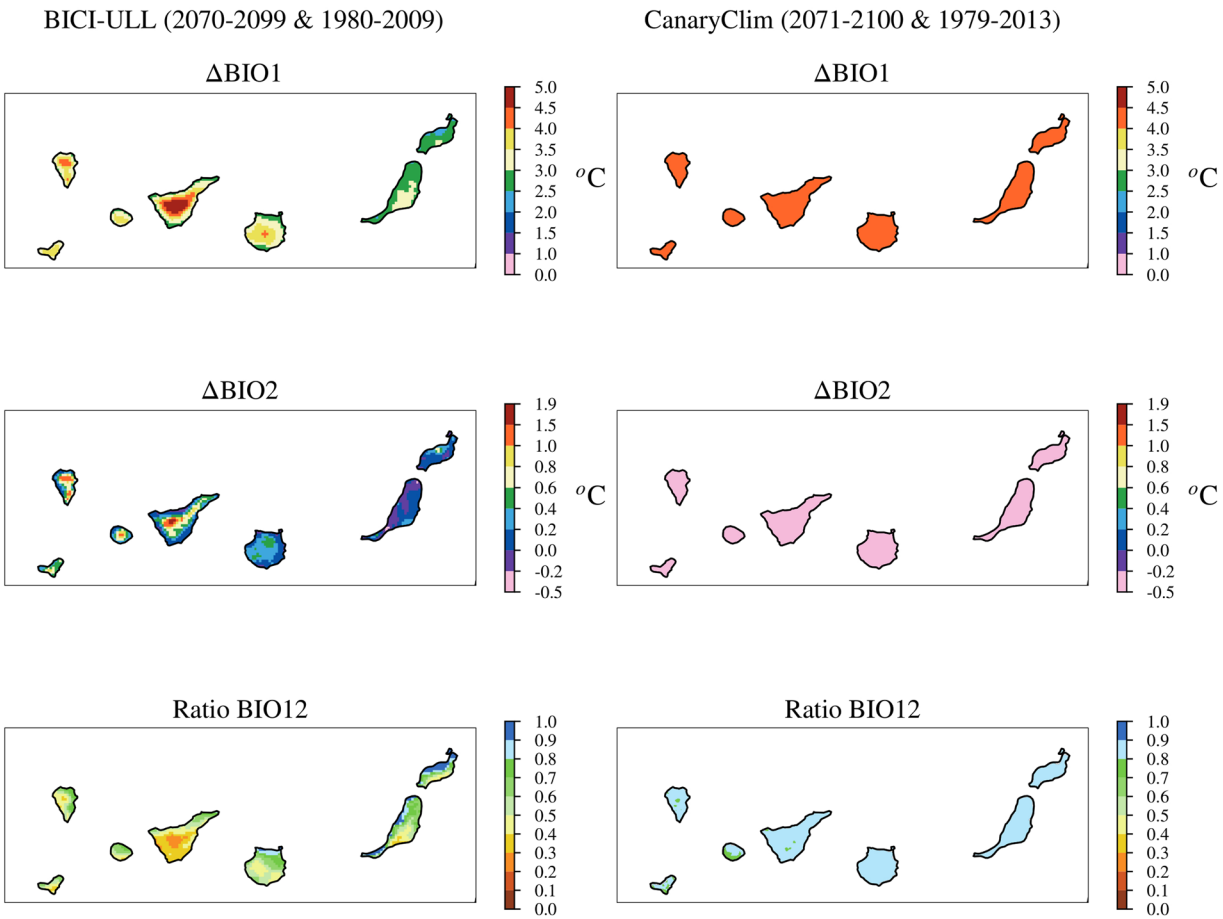

Fig. 7 Maps of projected changes in the Canary Islands of BIO1, BIO2, and BIO12 (from top to bottom) at the end 21st century for BICI–ULL (left panels) and CanaryClim v1.0[21] (right panels), corresponding to the scenarios RCP8.5 and SSP585, respectively. *ΔBIO1* represents the change in annual mean temperature, *ΔBIO2* indicates the change in mean temperature diurnal range, and *Ratio BIO12* refers to the annual precipitation ratio. The simulations are based on the IPSL–CM5A–MR WRF model for BICI–ULL and the IPSL–CM6A–LR for CanaryClim v1.0.

Temperature seems to exhibit a very similar behaviour to that of Atlas, while precipitation does not follow the same pattern. For grid points with higher precipitation, a noticeable difference is observed, as WorldClim 2.0 fails to reproduce the relationship between precipitation and orography. The precipitation range is approximately between 100 and 500 mm for WorldClim 2.0, whereas the Atlas shows precipitation exceeding 1300 mm in some areas. This discrepancy arises from the fact that WorldClim uses only 7 different observational sites in the Canary Islands[11], and none of them are located in the westernmost islands (El Hierro, La Palma, and La Gomera) which are among the rainiest in the archipelago. For instance, the island of La Palma has an average annual rainfall of 1000 mm in the highest areas.

Comparison of BICI-ULL with CanaryClim v1.0 datasets. As indicated previously, a dataset known as CanaryClim v1.0[21] has been recently published for the Canary Islands region, based on the methodology used for CHELSA[13,14] and characterised by a high spatial resolution (of the order of a hundred meters). This dataset presents very similar values to those of the Atlas for the recent past (comparison not shown), since both were produced from observations, although with slightly different interpolation methods. However, CanaryClim also provides data related to climate projections, which can be compared with those obtained in this study.

To highlight the importance of orography in this region, zonal averages have been performed. In particular, a transect has been selected on the island of Tenerife as depicted in Fig. 6. This island, the largest of the archipelago, was selected due to its orography, since this allows us to highlight the spatial inhomogeneities, such as the effect of the altitude or the differences between the southern and northern areas, the latter being more exposed to the trade winds. The study was conducted using the WRF simulation driven by the IPSL–CM5A–MR model for BICI–ULL and the data obtained from IPSL–CM6A–LR for CanaryClim v1.0. The plots represent the difference between the end-of-century projections (2070–2099 in BICI–ULL and 2071–2100 in CanaryClim v1.0) and the historical period (1980–2009 in BICI–ULL & 1979–2013 in CanaryClim v1.0) for temperature biovariables (BIO1 and BIO2), as well as the ratio between these periods for BIO12. The zonal mean terrain elevation for that transect is also plotted.

Additionally, Fig. 7 displays maps of future change (differences or ratios) for these biovariables across the Canary Islands. The findings indicate that the biovariables obtained from dynamic models (BICI–ULL) exhibit changes in biomarkers with altitude, whereas CanaryClim v1.0 suggests a uniform change, not dependent on the elevation of the grid point or on slope orientation, due to the low resolution of the data used to calculate the future changes. In addition, this low resolution and the independent consideration of the variables in the case of CanaryClim results in the loss of the physical relationships between the different variables. For example, the daily temperature range, BIO2, is influenced by many factors, including cloud cover, aerosols, precipitation, height of the planetary mixing layer, land cover type, etc.[49] A previous study[27] has shown that, in the Canary Islands, future raise in daily temperature range will be mainly influenced by a decrease in precipitation, which implies lower soil moisture and, therefore, a decrease in evaporative cooling. Thus, Fig. 6 shows that, for the BICI–ULL data, the biovariable BIO2 increases to a greater extent in the higher elevations, where the decrease in precipitation is stronger (BIO12). In GCMs the grid size is so large that each cell in the island's area is mainly composed of the sea, so the effect of changes in soil moisture are negligible.

For numerous biological or ecological studies, such as predicting the future likelihood of a species presence in a specific region of the Canary Islands, to understand how climate change depends on the topography is crucial. Databases based on a large number of observations, such as Atlas and CanaryClim, are a good starting point for studies for the recent past. However, for the estimation of future changes in areas with complex topography, the use of climate projections of much higher resolution than that of current GCMs would be desirable in order to consider the dependence of the expected changes on land features.

Usage Notes

Besides data sources for the dataset presented in this manuscript, data from further climate simulations can be integrated, e.g. additional data for the same region at a higher resolution can be obtained through interpolations that take into account the terrain's topography and specific properties of the Canary Islands. For any questions, suggestions or request of collaboration regarding BICI–ULL please contact the corresponding author.

Code availability

All the BICI–ULL calculations were conducted exploiting NetCDF4 data manipulation and analysis tools. CDO (Climate Data Operators), Python, and bash language were used as principal environments. Commands and scripts are available through the ULL research data repository website in Sosa-Guillén *et al.*[26].

Received: 3 April 2024; Accepted: 14 November 2024;
Published online: 04 December 2024

References

1. The intergovernmental panel on climate change (IPCC). https://www.ipcc.ch/ Accessed on 16 February 2024 (2024).
2. Lee, H. *et al*. Ipcc, 2023: Climate change 2023: Synthesis report, summary for policymakers. contribution of working groups i, ii and iii to the sixth assessment report of the intergovernmental panel on climate change [Core Writing Team, H. Lee and J. Romero (eds.)]. IPCC, Geneva, Switzerland. IPCC https://doi.org/10.59327/IPCC/AR6-9789291691647.001 (2023).
3. Nurse, L. A. *et al*. Small islands, https://hal.science/hal-01090732 (2014).
4. Lima, M. Â. M.On the impacts of tropical cyclones in the Northeastern Atlantic. Ph.D. thesis, Universidade de Lisboa http://hdl.handle.net/10451/56717 (2023).
5. Carrillo, J., Pérez, J., Expósito, F., Díaz, J. & González, A. Projections of wildfire weather danger in the Canary Islands. *Scientific reports* **12**, 8093, https://doi.org/10.1038/s41598-022-12132-5 (2022).
6. Bramwell, D. Conserving biodiversity in the Canary Islands. *Annals of the Missouri Botanical Garden* 28–37, https://doi.org/10.2307/2399622 (1990).
7. Zachow, C. *et al*. Fungal diversity in the rhizosphere of endemic plant species of Tenerife (Canary Islands): relationship to vegetation zones and environmental factors. *The ISME journal* **3**, 79–92, https://doi.org/10.1038/ismej.2008.87 (2009).
8. Charalampopoulos, I., Droulia, F., Kokkoris, I. P. & Dimopoulos, P. Future bioclimatic change of agricultural and natural areas in Central Europe: An ultra-high resolution analysis of the De Martonne index. *Water* **15**, https://doi.org/10.3390/w15142563 (2023).
9. Proćków, M., Konowalik, K. & Proćków, J. Contrasting effects of climate change on the european and global potential distributions of two mediterranean helicoid terrestrial gastropods. *Regional Environmental Change* **19**, 2637–2650, https://doi.org/10.1007/s10113-019-01573-w (2019).
10. Fourcade, Y., Engler, J. O., Rödder, D. & Secondi, J. Mapping species distributions with MAXENT using a geographically biased sample of presence data: a performance assessment of methods for correcting sampling bias. *PloS one* **9**, e97122, https://doi.org/10.1371/journal.pone.0097122 (2014).
11. Fick, S. E. & Hijmans, R. J. WorldClim 2: new 1-km spatial resolution climate surfaces for global land areas. *International journal of climatology* **37**, 4302–4315, https://doi.org/10.1002/joc.5086 (2017).
12. Hijmans, R. J., Cameron, S. E., Parra, J. L., Jones, P. G. & Jarvis, A. Very high resolution interpolated climate surfaces for global land areas. *International Journal of Climatology: A Journal of the Royal Meteorological Society* **25**, 1965–1978, https://doi.org/10.1002/joc.1276 (2005).
13. Karger, D. N. *et al*. Climatologies at high resolution for the earth's land surface areas. *Scientific data* **4**, 1–20, https://doi.org/10.1038/sdata.2017.122 (2017).
14. Brun, P., Zimmermann, N. E., Hari, C., Pellissier, L. & Karger, D. N. Global climate-related predictors at kilometer resolution for the past and future. *Earth System Science Data* **14**, 5573–5603, https://doi.org/10.5194/essd-14-5573-2022 (2022).
15. Noce, S., Caporaso, L. & Santini, M. A new global dataset of bioclimatic indicators. *Scientific data* **7**, 398, https://doi.org/10.1038/s41597-020-00726-5 (2020).
16. Noce, S., Caporaso, L.Santini, M. CMCC-BioClimInd. A new global dataset of bioclimatic indicators [dataset]. *Fondazione Centro Euromediterraneo sui Cambiamenti Climatici, PANGAEA*, https://doi.org/10.1594/PANGAEA.904278 (2019).
17. Kriticos, D. J. *et al*. CliMond: global high-resolution historical and future scenario climate surfaces for bioclimatic modelling. *Methods in Ecology and Evolution* **3**, 53–64, https://doi.org/10.1111/j.2041-210X.2011.00134.x (2012).
18. Kriticos, D. J., Jarovsik, V. & Ota, N. Extending the suite of bioclim variables: a proposed registry system and case study using principal components analysis. *Methods in Ecology and Evolution* **5**, 956–960, https://doi.org/10.1111/2041-210X.12244 (2014).

19. Abatzoglou, J. T., Dobrowski, S. Z., Parks, S. A. & Hegewisch, K. C. TerraClimate, a high-resolution global dataset of monthly climate and climatic water balance from 1958–2015. *Scientific data* **5**, 1–12, https://doi.org/10.1038/sdata.2017.191 (2018).
20. O'Neill, B. C. *et al*. The scenario model intercomparison project (ScenarioMIP) for CMIP6. *Geoscientific Model Development* **9**, 3461–3482, https://doi.org/10.5194/gmd-9-3461-2016 (2016).
21. Patiño, J. *et al*. Spatial resolution impacts projected plant responses to climate change on topographically complex islands. *Diversity and Distributions* https://doi.org/10.1111/ddi.13757 (2023).
22. Unser, M., Aldroubi, A. & Eden, M. B-spline signal processing. i. theory. *IEEE transactions on signal processing* **41**, 821–833, https://doi.org/10.1109/78.193220 (1993).
23. Bedia, J., Herrera, S. & Gutiérrez, J. M. Dangers of using global bioclimatic datasets for ecological niche modeling. limitations for future climate projections. *Global and Planetary Change* **107**, 1–12, https://doi.org/10.1016/j.gloplacha.2013.04.005 (2013).
24. Carrillo, J. *et al*. The uneven impact of climate change on drought with elevation in the Canary Islands. *npj Climate and Atmospheric Science* **6**, 31, https://doi.org/10.1038/s41612-023-00358-7 (2023).
25. Perez, J. C., Exposito, F. J., Gonzalez, A. & Diaz, J. P. Climate projections at a convection-permitting scale of extreme temperature indices for an archipelago with a complex microclimate structure. *Weather and Climate Extremes* **36**, 100459, https://doi.org/10.1016/j.wace.2022.100459 (2022).
26. Sosa-Guillén, P., Exposito, F. J., Pérez Darias, J. C., González, A. & Diaz, J. P. BICI-ULL: Bioclimatic indicators dataset for the orographically complex Canary Islands archipelago, https://doi.org/10.17632/pppj6cbtkc.1 (2024). Data set.
27. Expósito, F. J., González, A., Pérez, J. C., Díaz, J. P. & Taima, D. High-resolution future projections of temperature and precipitation in the Canary Islands. *Journal of Climate* **28**, 7846–7856, https://doi.org/10.1175/JCLI-D-15-0030.1 (2015).
28. Pérez, J. *et al*. Evaluation of WRF parameterizations for dynamical downscaling in the Canary Islands. *Journal of climate* **27**, 5611–5631, https://doi.org/10.1175/JCLI-D-13-00458.1 (2014).
29. Lim, K.-S. S. & Hong, S.-Y. Development of an effective double-moment cloud microphysics scheme with prognostic cloud condensation nuclei (CCN) for weather and climate models. *Monthly weather review* **138**, 1587–1612, https://doi.org/10.1175/2009MWR2968.1 (2010).
30. Hong, S.-Y., Noh, Y. & Dudhia, J. A new vertical diffusion package with an explicit treatment of entrainment processes. *Monthly weather review* **134**, 2318–2341, https://doi.org/10.1175/MWR3199.1 (2006).
31. Chen, F. & Dudhia, J. Coupling an advanced land surface–hydrology model with the Penn State–NCAR MM5 modeling system. part i: model implementation and sensitivity. *Monthly weather review* **129**, 569–585 (2001).
32. Collins, W. D. *et al*. Description of the NCAR community atmosphere model (CAM 3.0). *NCAR Tech. Note NCAR/TN-464+ STR* **226**, 1326–1334 (2004).
33. Kain, J. S. The Kain–Fritsch convective parameterization: an update. *Journal of applied meteorology* **43**, 170–181 (2004).
34. McSweeney, C. F., Jones, R. G., Lee, R. W. & Rowell, D. P. Selecting CMIP5 GCMs for downscaling over multiple regions. *Climate Dynamics* **44**, 3237–3260, https://doi.org/10.1007/s00382-014-2418-8 (2015).
35. Van Vuuren, D. P. *et al*. The representative concentration pathways: an overview. *Climatic change* **109**, 5–31, https://doi.org/10.1007/s10584-011-0148-z (2011).
36. Christensen, J. H., Boberg, F., Christensen, O. B. & Lucas-Picher, P. On the need for bias correction of regional climate change projections of temperature and precipitation. Geophysical research letters **35**, https://doi.org/10.1029/2008GL035694 (2008).
37. Switanek, M. B. *et al*. Scaled distribution mapping: a bias correction method that preserves raw climate model projected changes. *Hydrology and Earth System Sciences* **21**, 2649–2666, https://doi.org/10.5194/hess-21-2649-2017 (2017).
38. Leuprecht, A. & Zumstein, P. PyCAT: A Python library for climate analysis. GitHub,Wegener Center for Climate and Global Change, University of Graz. https://github.com/wegener-center/pyCAT (2015).
39. Pérez, J. C., González, A., Díaz, J. P., Expósito, F. J. & Felipe, J. Climate change impact on future photovoltaic resource potential in an orographically complex archipelago, the Canary Islands. *Renewable Energy* **133**, 749–759, https://doi.org/10.1016/j.renene.2018.10.077 (2019).
40. González, A., Pérez, J. C., Díaz, J. P. & Expósito, F. J. Future projections of wind resource in a mountainous archipelago, Canary Islands. *Renewable Energy* **104**, 120–128, https://doi.org/10.1016/j.renene.2016.12.021 (2017).
41. Ellenberg, H.Vegetation Mitteleuropas (Ulmer, 1963).
42. Rivas-Martínez, S., Rivas-Saenz, S., Penas, A. *et al*. Worldwide Bioclimatic Classification System (Backhuys Pub. Kerkwerve, The Netherlands, 2002).
43. Hargreaves, G. H. & Samani, Z. A. Estimating potential evapotranspiration. *Journal of the irrigation and Drainage Division* **108**, 225–230, https://doi.org/10.1061/JRCEA4.0001390 (1982).
44. Hargreaves, G. H. & Allen, R. G. History and evaluation of Hargreaves evapotranspiration equation. *Journal of irrigation and drainage engineering* **129**, 53–63, https://doi.org/10.1061/(ASCE)0733-9437(2003)129:1(53) (2003).
45. Thornthwaite, C. W. An approach toward a rational classification of climate. *Geographical review* **38**, 55–94, https://doi.org/10.2307/210739 (1948).
46. Mayer, P., Luque, A. & García-Hernández, F. Atlas climático interactivo de canarias de alta resolución espacial. fuentes de datos, metodología y resultados., Grupo de Geografía Física y Medio Ambiente de la ULPGC, Grafcan, SA y Consejería de Transición Ecológica Lucha contra el Cambio Climático y Planificación Territorial del Gobierno autónomo de Canarias. https://atlasclimatico.sitcan.es/ (2021).
47. Luque Söllheim, Á. L., Máyer Suarez, P. & García Hernández, F. The digital climate atlas of the Canary Islands: A tool to improve knowledge of climate and temperature and precipitation trends in the Atlantic islands. *Climate Services* **34**, 100487, https://doi.org/10.1016/j.cliser.2024.100487 (2024).
48. Jones, P. W. First-and second-order conservative remapping schemes for grids in spherical coordinates. *Monthly Weather Review* **127**, 2204–2210, https://doi.org/10.1175/1520-0493(1999)127_2204:FASOCR_2.0.CO;2 (1999).
49. Zhong, Z. *et al*. Reversed asymmetric warming of sub-diurnal temperature over land during recent decades. *Nature Communications* **14**, 7189, https://doi.org/10.1038/s41467-023-43007-6 (2023).
50. Dunne, J. P. *et al*. GFDL's ESM2 global coupled climate–carbon earth system models. part i: Physical formulation and baseline simulation characteristics. *Journal of climate* **25**, 6646–6665, https://doi.org/10.1175/JCLI-D-11-00560.1 (2012).
51. Dufresne, J.-L. *et al*. Climate change projections using the IPSL-CM5 earth system model: from CMIP3 to CMIP5. *Climate dynamics* **40**, 2123–2165, https://doi.org/10.1007/s00382-012-1636-1 (2013).
52. Watanabe, S. *et al*. MIROC-ESM 2010: Model description and basic results of CMIP5-20c3m experiments. *Geoscientific Model Development* **4**, 845–872, https://doi.org/10.5194/gmd-4-845-2011 (2011).

Acknowledgements

Acknowledgments are expressed to the World Climate Research Programme's Working Group on Coupled Modelling, to the CMCC-BioClimInd research project, to the GFyMA group (especially to professors Pablo Mayer, Fabián García, and Ángel De Luque), and to the climate modeling groups (listed in Table 1) for producing and making available their model output. The authors also thank the Government of the Canary Islands, *Consejería de Transición Ecológica, Lucha contra el Cambio Climático y Planificación Territorial*, for their support (published agreement: B.O.C. No. 238, November 20, 2020), and the PLANCLIMAC2 Project (1/

MAC/2/2.4/0006) for its support. This Project has been financed by the European Union INTERREG MAC 2021-2027 Program. Part of this work has also been funded by the CanBio project. Also, they thank the Government of the Canary Islands, Consejería de Transición Ecológica y Energía, for their support (within the framework of the cooperation agreement signed on November 08, 2024).

Author contributions

P.S. designed the research, created the data, created the figures and tables, wrote the paper; A.G. provided the input climatic data, wrote the paper; J.P. provided the input climatic data, wrote the paper; F.E. provided the input climatic data, wrote the paper; J.D. provided the input climatic data, designed the research, wrote the paper. All authors reviewed the manuscript.

Competing interests

The authors declare no competing interests.

Additional information

Supplementary information The online version contains supplementary material available at https://doi.org/10.1038/s41597-024-04134-x.

Correspondence and requests for materials should be addressed to P.S.-G.